



# Reproducibility of Standardized Uptake Values Including Volume Metrics Between TOF-PET-MR and TOF-PET-CT

Aruki Tanaka<sup>1</sup>, Tetsuro Sekine<sup>1,2,3,4\*</sup>, Edwin E. G. W. ter Voert<sup>3,4</sup>, Konstantinos G. Zeimpekis<sup>3,4,5</sup>, Gaspar Delso<sup>6</sup>, Felipe de Galiza Barbosa<sup>3,4</sup>, Geoffrey Warnock<sup>3,4,7</sup>, Shin-ichiro Kumita<sup>1</sup>, Patrick Veit Haibach<sup>3,4,8,9</sup> and Martin Huellner<sup>3,4</sup>

<sup>1</sup> Department of Radiology, Nippon Medical School Hospital, Tokyo, Japan, <sup>2</sup> Department of Radiology, Nippon Medical School Musashi Kosugi Hospital, Kanagawa, Japan, <sup>3</sup> Departments of Nuclear Medicine, University Hospital Zurich, Zurich, Switzerland, <sup>4</sup> University of Zurich, Zurich, Switzerland, <sup>5</sup> Department of Nuclear Medicine, Inselspital, Bern University Hospital, University of Bern, Bern, Switzerland, <sup>6</sup> GE Healthcare, Waukesha, WI, United States, <sup>7</sup> PMOD Technologies Ltd., Zurich, Switzerland, <sup>8</sup> Toronto Joint Department Medical Imaging, University Health Network, Sinai Health System, Women's College Hospital, Toronto, ON, Canada, <sup>9</sup> Department of Medical Imaging, University of Toronto, Toronto, ON, Canada

## OPEN ACCESS

### Edited by:

Giorgio Treglia,  
Ente Ospedaliero Cantonale  
(EOC), Switzerland

### Reviewed by:

Maria Mathew D'Souza,  
Institute of Nuclear Medicine & Allied  
Sciences (DRDO), India  
Luca Camoni,  
University of Brescia, Italy

### \*Correspondence:

Tetsuro Sekine  
tetsuro.sekine@gmail.com

### Specialty section:

This article was submitted to  
Nuclear Medicine,  
a section of the journal  
Frontiers in Medicine

Received: 15 October 2021

Accepted: 07 February 2022

Published: 02 March 2022

### Citation:

Tanaka A, Sekine T, ter Voert EEGW, Zeimpekis KG, Delso G, de Galiza Barbosa F, Warnock G, Kumita S-i, Veit Haibach P and Huellner M (2022) Reproducibility of Standardized Uptake Values Including Volume Metrics Between TOF-PET-MR and TOF-PET-CT. *Front. Med.* 9:796085. doi: 10.3389/fmed.2022.796085

**Purpose:** To investigate the reproducibility of tracer uptake measurements, including volume metrics, such as metabolic tumor volume (MTV) and tumor lesion glycolysis (TLG) obtained by TOF-PET-CT and TOF-PET-MR.

**Materials and Methods:** Eighty consecutive patients with different oncologic diagnoses underwent TOF-PET-CT (Discovery 690; GE Healthcare) and TOF-PET-MR (SIGNA PET-MR; GE Healthcare) on the same day with single dose—18F-FDG injection. The scan order, PET-CT following or followed by PET-MR, was randomly assigned. A spherical volume of interest (VOI) of 30 mm was placed on the liver in accordance with the PERCIST criteria. For liver, the maximum and mean standard uptake value for body weight (SUV) and lean body mass (SUL) were obtained. For tumor delineation, VOI with a threshold of 40 and 50% of SUVmax was used (VOI40 and VOI50). The SUVmax, SUVmean, SUVpeak, MTV and TLG were calculated. The measurements were compared between the two scanners.

**Results:** In total, 80 tumor lesions from 35 patients were evaluated. There was no statistical difference observed in liver regions, whereas in tumor lesions, SUVmax, SUV mean, and SUVpeak of PET-MR were significantly underestimated ( $p < 0.001$ ) in both VOI40 and VOI50. Among volume metrics, there was no statistical difference observed except TLG on VOI50 ( $p = 0.03$ ). Correlation between PET-CT and PET-MR of each metrics were calculated. There was a moderate correlation of the liver SUV and SUL metrics ( $r = 0.63$ – $0.78$ ). In tumor lesions, SUVmax and SUVmean had a stronger correlation with underestimation in PET-MR on VOI 40 (SUVmax and SUVmean;  $r = 0.92$  and  $0.91$  with slope =  $0.71$  and  $0.72$ , respectively). In the evaluation of MTV and TLG, the stronger correlations were observed both on VOI40 (MTV and TLG;  $r = 0.75$  and  $0.92$ ) and VOI50 (MTV and TLG;  $r = 0.88$  and  $0.95$ ) between PET-CT and PET-MR.

**Conclusion:** PET metrics on TOF-PET-MR showed a good correlation with that of TOF-PET-CT. SUV<sub>max</sub> and SUV<sub>peak</sub> of tumor lesions were underestimated by 16% on PET-MRI. MTV with % threshold can be regarded as identical volumetric markers for both TOF-PET-CT and TOF-PET-MR.

**Keywords:** PET/MR, PET/CT, reproducibility, metabolic tumor volume, FDG-F production 18, TOF (time-of-flight), SUV

## INTRODUCTION

18F-fluorodeoxyglucose (FDG) positron emission tomography (PET) is used routinely in the diagnosis, staging, restaging, and treatment monitoring of various cancers (1). The maximum standardized uptake value (SUV<sub>max</sub>) remains the main uptake measurement parameters of tumors, owing to its simplicity and high reproducibility. In order to achieve a more detailed assessment of tumor characteristics, recent studies have focused on demonstrating the prognostic value of positron emission tomography (PET)-based volumetric parameters, such as metabolic tumor volume (MTV) and total lesion glycolysis (TLG) (2–6). MTV is defined as the sum of the volume of voxels, and TLG is the product of the MTV and SUV<sub>mean</sub>. These indicators can be used for prognostication as they reflect the activity of glucose metabolism in the entire tumor compared to SUV<sub>max</sub> which only reflects a single voxel value.

Following the success of the positron emission tomography and computed tomography (PET-CT) system, integrated PET and magnetic resonance (PET-MR) systems have been clinically introduced and the number of these scanners is gradually increasing worldwide (7–10). In clinical or research settings, several PET machines were used for identical clinical and research purposes. In such a situation, reproducibility among scanners remains an issue to be solved (11, 12). Especially on PET-MR, the error derived from the attenuation correction based on MRI (MRAC) impairs its reproducibility (13–23). Several studies have been conducted to assess the impact of this impairment. In these studies, the metrics of max, mean, or peak SUVs were mainly evaluated (24–26); however, the studies on the correlations of MTV and TLG between PET-CT and PET-MR are still very limited (27–31). Specifically, in the case of time-of-flight (TOF)-PET-MR instruments, no study has evaluated the volumetric parameters. In these machines, the effect of the MRAC error is reduced by TOF-reconstruction (32–34).

In this study, we aimed to determine the TOF-PET-CT and TOF-PET-MR reproducibility of FDG PET-SUV measurements, including volumetric metrics obtained by PET-CT and PET-MR examinations performed on the same day in oncologic patients.

## MATERIALS AND METHODS

### Ethical Statement

Patients were enrolled in this retrospective study as part of a larger prospective study (NCT02316431). All patients provided written informed consent prior to their inclusion in the study.

### Study Subjects

Eighty consecutive patients with different oncologic disease underwent 18F-FDG PET-CT and 18F-FDG PET-MR. All examinations were performed on the same day with a single injection of FDG. The inclusion criteria called for patients with visible tumors both on PET-CT and PET-MR. The scan interval between both examinations was <70 min. A sufficient tracer activity was maintained to generate PET images on PET-MR equivalent to a 70% dose of PET-CT (35).

### Image Acquisition

PET-CT acquisition followed a standard protocol for clinical oncologic imaging on a TOF-PET-CT scanner (Discovery 690; GE Healthcare, Waukesha, Wisconsin, USA) (12). The whole-body PET data were acquired in 3D TOF mode with a scan duration of 2 min per bed position, an axial FOV of 153 mm, and 23% overlap of bed positions—resulting in a total PET acquisition time of 16–20 min. Standard CT was acquired for diagnostic purposes and CT attenuation correction (CTAC).

For the PET-MR imaging examination, we used a simultaneous TOF-PET-MR system, which comprised a 3.0-T whole-body MR imaging system and SiPM PET detectors (SIGNA PET-MR; GE Healthcare, Waukesha, Wisconsin, USA). Whole-body list-mode PET data were acquired in 3D TOF mode with a scan duration of 2–4 min per bed position. The scan time per bed position depended on the imaging protocol selected according to clinical indication. An axial FOV of 250 mm and a 24% overlap of bed positions were used, resulting in a total PET acquisition time of 12–24 min. During PET-MR imaging, a 3D liver acquisition with volume acquisition (LAVA Flex) T1-weighted pulse sequence (repetition time—~4 ms; echo time—2.23 ms; flip angle—5°; section thickness—5.2 mm with 2.6 mm overlap; 120 sections; pixel size—1.95 × 1.95 mm<sup>2</sup>, partial Fourier—70.3%; and acquisition time—18 s per bed position) was acquired for MRAC (33, 36). Additionally, different anatomic MR pulse sequences were also used for diagnostic imaging.

### Imaging Reconstruction

The reconstruction parameters of PET images on PET-CT and PET-MR were selected to be as similar as possible. The detailed parameters were described elsewhere (35). In PET-CT, a fully 3D OSEM iterative reconstruction, including PSF compensation with three iterations and 18 subsets and a 256 × 256 image grid (2.73 × 2.73 × 3.27-mm voxels), was used. In PET-MR imaging, OSEM, including PSF compensation with three iterations and 16 subsets, and a 256 × 256 image grid (2.34 × 2.34 × 2.78-mm voxels), was used for reconstruction of the PET images. In both systems, transaxial post-reconstruction Gaussian filter

4 mm, axial filter 1:4:1, normalization, random, scatter, dead-time and decay correction were applied. The parameters of PET-CT had been fixed as clinical scan. The minor difference of parameters between both scanners were due to the restriction by the vendor. We could not choose the parameter freely but one out of several options. Both PET image datasets were generated by TOF calculation. CTAC was used to generate PET on PET-CT and MRAC for PET on PET-MR. To compensate for the difference in sensitivity between the two scanners derived from SiPM detectors on PET-MR, we retrospectively un-listed the list mode PET data on PET-MR and generated 70% simulated-dose PET-MR images comparable to PET-CT (35).

## Imaging Analysis

We extracted normal liver regions and oncologic lesions for further evaluation. As normal liver regions, the liver mean SUV (SUVmean) normalized to lean body mass (SULmean) was measured. These values have been proposed as a quality control measure for FDG PET-CT in solid tumors (PERCIST) 2.0 (12). A VOI with a diameter of 3 cm was manually drawn on the right lobe of the liver to analyze the concordance between PET-CT and PET-MR.

As target lesions, a maximum of three tumors were extracted per each of the four body parts (head and neck, chest, upper abdomen, and pelvis) by two independent board-certified radiologists (T.S and B.F). Tumors larger than 25 mL were excluded to maintain stability in the statistical analysis. We also excluded target lesions that could not reliably be delineated from physiological uptake (such as the heart, kidney, and bladder).

The volume-of-interest (VOI) was defined by manually drawing polygonal VOIs to enclose the entire tumor with sufficient margins on every slice where the target tumor was seen. Physiological uptake was carefully avoided. In this study, we used the fixed 40 and 50% to SUVmax threshold method (VOI40 and VOI50, respectively), which is a procedure for defining the area of the tumor as a region with a higher SUV than a certain percentage of the SUVmax within the tumor (12).

We used PMOD (version 4.0; PMOD Inc., Zurich, Switzerland) for VOI segmentation and calculation of SUVmax, SUVpeak, SUVmean, MTV, and TLG. VOIs below 1 mL were excluded for the static of peak (37).

## Statistical Analysis

We performed the Kolmogorov–Smirnov test for the continuous variables. The values of liver SUV and SUL were normally distributed and listed as mean  $\pm$  standard deviation. The values of tumor SUV were not normally distributed and listed as median and interquartile range (IQR). To clarify the difference in PET metrics between the two scanners, we performed a paired *t*-test for normally distributed variables and Wilcoxon signed-rank test for not normally distributed variables, respectively. In order to prove the correlation between the two scanners, Pearson's test was performed for these metrics as well. To visualize the deviation of the difference, Bland–Altman plots with limits of agreement were generated (38). Statistical significance was set

**TABLE 1 |** Demographic and clinical data.

Age in years, mean $\pm$ SD (range)	63.1 $\pm$ 10.7 (40–84)
Body height in meters, mean $\pm$ SD (range)	1.7 $\pm$ 0.1 (1.49–1.9)
Body weight in kilograms, mean $\pm$ SD (range)	71.7 $\pm$ 15.2 (44–110)
BMI, mean $\pm$ SD (range)	24.5 $\pm$ 4.1 (17.4–32.7)
Injected dose in MBq/kg, mean $\pm$ SD (range)	3.20 $\pm$ 0.30 (2.84–4.07)
Gender ( <i>n</i> )	
Male	22
Female	13
Clinical indication ( <i>n</i> )	
Head and neck cancer	9
Lung cancer	8
Pancreatic cancer	3
Breast cancer	2
Esophageal cancer	2
Rectal cancer	2
Cancer of unknown primary	2
Malignant lymphoma	2
Colon cancer	2
Intrahepatic cholangiocarcinoma	1
Multiple myeloma	1
Malignant melanoma	1
PET-MR images acquired after injection in minutes, mean $\pm$ SD (range)	75 $\pm$ 12 (46–104)
PET-CT images acquired after injection in minutes, mean $\pm$ SD (range)	63 $\pm$ 26 (37–144)
Scan interval (PET-MR minus PET-CT) (min), mean $\pm$ SD (range)	–12 $\pm$ 32 (–54–68)

at  $p < 0.05$ . Statistical analyses were performed using SPSS Statistics, version 19.0.0 (IBM, Armonk, NY, USA).

## RESULTS

A total of 35 patients with 80 tumor lesions were included. The detailed information is given in **Table 1**. The mean and standard deviation of each metric on both PET-CT and PET-MR is given in **Table 2**. There was no statistical difference observed in the liver regions, whereas the tumor SUVmax, and SUVpeak of PET-MR were significantly underestimated ( $p < 0.001$ ). Among volume metrics consisting of MTV and TLG, there was no statistical difference observed except for the TLG of VOI50 ( $p = 0.03$ ). The correlation analysis between PET-CT and PET-MR is given in **Table 3**. The correlation of the liver SUVs and SULs was moderate ( $r = 0.63$ – $0.78$ ) (**Figures 1A–D**). In tumor lesions, SUVmax, SUVmean, and SUVpeak were strongly correlated with an underestimation on PET-MR ( $r = 0.92$ ,  $0.91$ , and  $0.95$ , respectively; slope =  $0.71$ ,  $0.72$ , and  $0.79$ , respectively) (**Figures 2A–D**). For MTV and TLG, high correlations were observed with slightly better results on VOI50 compared to VOI40 ( $0.88$  and  $0.95$  vs.  $0.75$  and  $0.92$ , respectively) (**Figures 3A–D**). The results of the Bland–Altman analysis are presented in **Table 4**. Mean differences of all measurements were negative except MTV in VOI40 and

**TABLE 2** | Details of SUV measurements in liver and tumor lesions.

			PET-CT mean $\pm$ SD	PET-MR mean $\pm$ SD	P (paired <i>t</i> -test)
Liver	SUVmax		3.63 $\pm$ 0.70	3.48 $\pm$ 0.84	0.17
	SUVmean		2.21 $\pm$ 0.35	2.13 $\pm$ 0.47	0.14
	SULmax		2.74 $\pm$ 0.44	2.64 $\pm$ 0.61	0.22
	SULmean		1.67 $\pm$ 0.20	1.61 $\pm$ 0.30	0.16
			PET-CT median $\pm$ IQR	PET-MR median $\pm$ IQR	(Wilcoxon signed-rank test)
Tumor lesion	VOI40	SUVmax	9.54 (6.32–14.09)	8.23 (5.62–12.18)	<0.001
		SUVpeak	6.11 (3.80–9.24)	4.98 (3.44–7.92)	<0.001
		SUVmean	5.92 (4.09–8.57)	5.07 (3.52–7.31)	<0.001
		MTV	2.30 (0.78–6.15)	2.34 (0.92–5.97)	0.850
		TLG	15.35 (4.07–31.38)	12.42 (4.07–38.60)	0.002
	VOI50	SUVmean	6.57 (4.94–9.38)	5.60 (4.04–8.13)	<0.001
		MTV	1.42 (0.45–2.87)	1.50 (0.59–3.43)	0.694
		TLG	9.54 (2.80–21.75)	8.10 (2.67–23.02)	0.002

**TABLE 3** | The result of linear regression analysis where x-axis is PET/MR measurements and y-axis is PET/CT measurements.

			Slope	Intercept	r
Liver	SUVmax		0.83	0.45	0.69
	SUVmean		1.05	−0.19	0.78
	SULmax		0.89	0.21	0.63
	SULmean		0.99	−0.04	0.64
Tumor lesion	VOI40	SUV max	0.71	1.48	0.92
		SUVpeak	0.80	0.35	0.94
		SUVmean	0.72	0.87	0.91
		MTV	0.92	0.68	0.75
	VOI50	TLG	0.85	1.24	0.92
		SUVmean	0.71	0.95	0.93
		MTV	0.90	0.35	0.88
		TLG	0.84	0.98	0.95

VOI50 (Figures 1E–H, 2E–H, 3E–H). The representative cases are shown in Figures 4, 5.

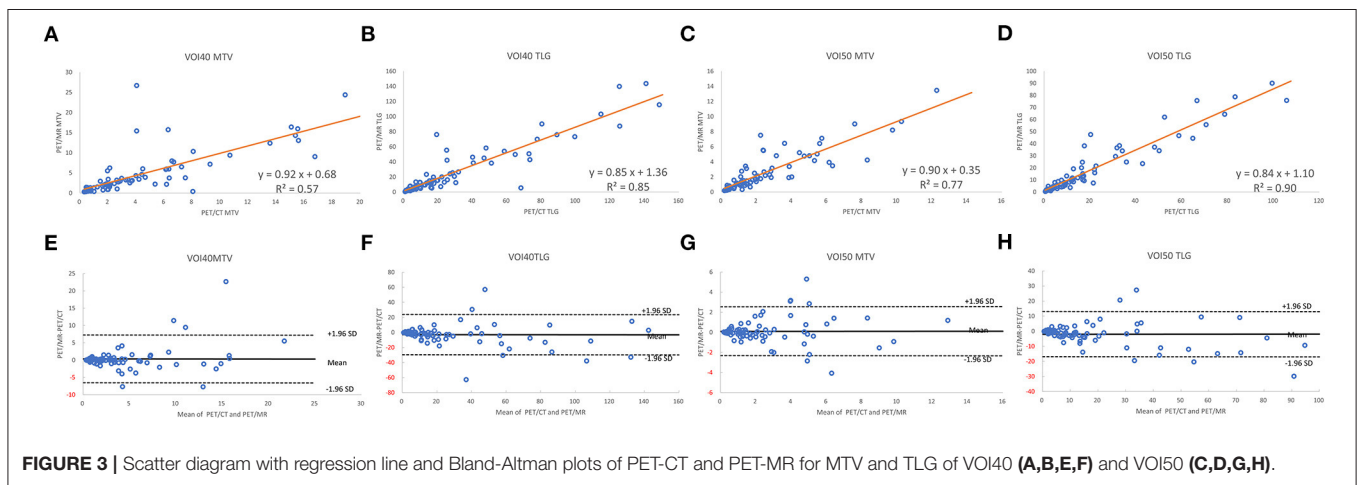
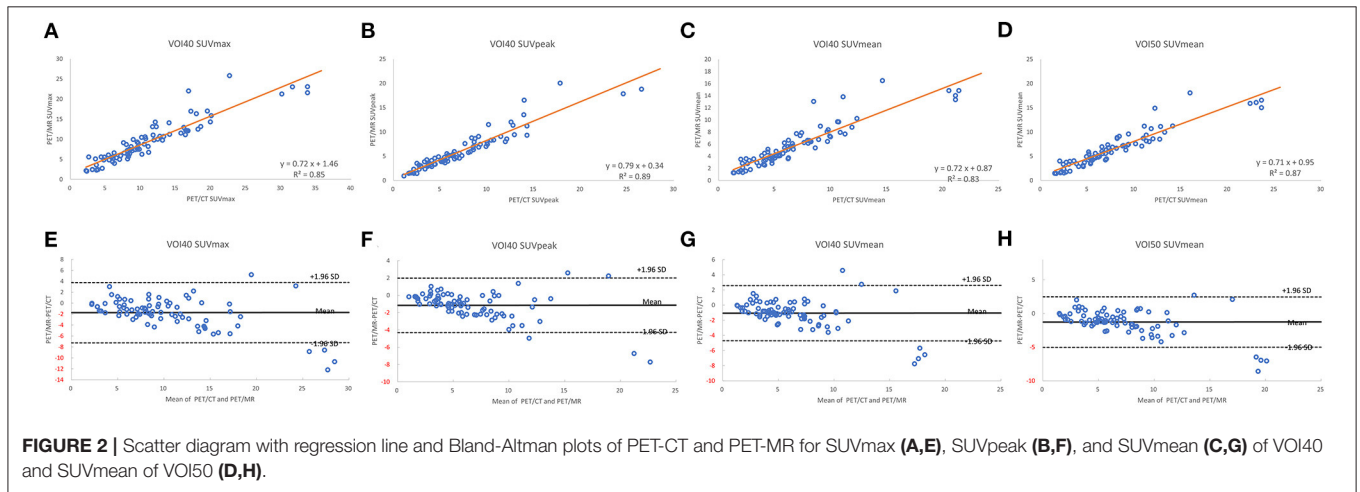
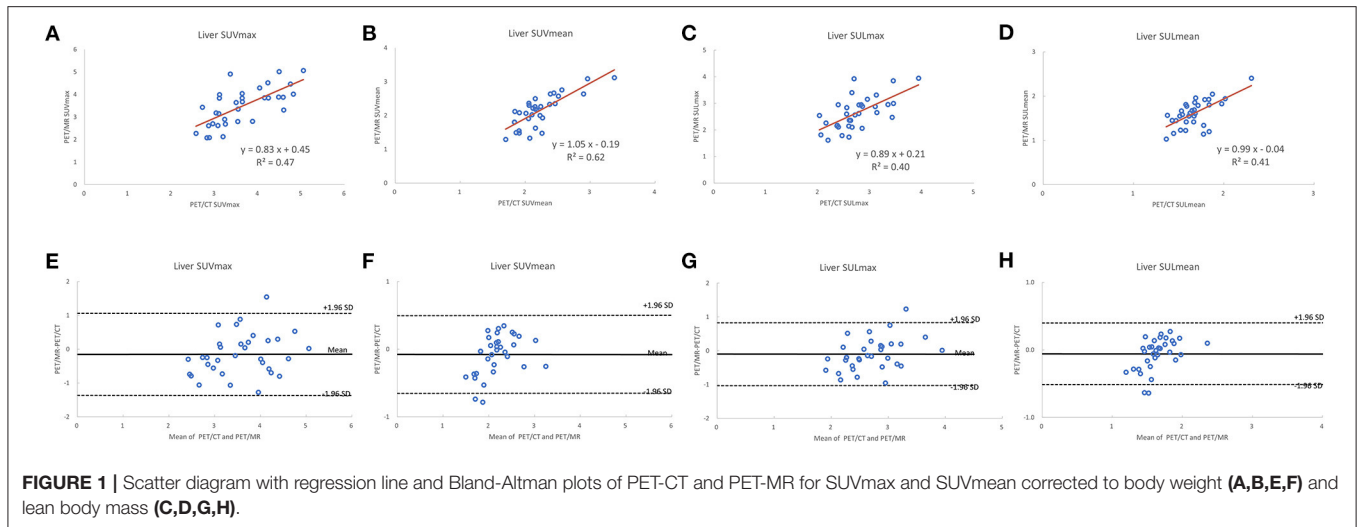
## DISCUSSION

This study demonstrated that SUV measurements correlate well between PET-MR and PET-CT. SUVmax and SUVmean of the reference area, liver regions, were not under- or overestimated on PET-MR. However, the SUVmax, SUVpeak, and SUVmean of tumor lesions were underestimated by  $\sim$ 16%. Fortunately, MTV was maintained between both scanners.

There are notable strengths to the current study. First, we evaluated the reproducibility of volume metrics between PET-CT and PET-MR, which was evaluated only by the sole previous study where non-TOF-PET-MR machines were used (27). TOF-reconstruction clearly compensates

for the error from the MRAC (32, 33). For this reason, their results cannot be transferred to a TOF-PET-MR machine, but separate analysis is required. Second, the scan order, PET-MR following or followed by PET-CT, was randomly in our study. Delayed uptake is a critical issue when comparing the reproducibility (39). Third, we generated PET images on PET-MR equivalent to a 70% dose of PET-CT. The higher sensitivity of SiPM detectors or novel reconstruction techniques can influence PET metrics (40, 41). For a fair comparison regardless of detector sensitivity, we developed the current study design.

Although the extent of the difference was within the limit of repeatability (i.e., 25%) (42), a significant underestimation of several parameters was observed on PET-MR. The underestimation of SUVmax, mean, and peak is expected to be derived from two factors. One is that incomplete

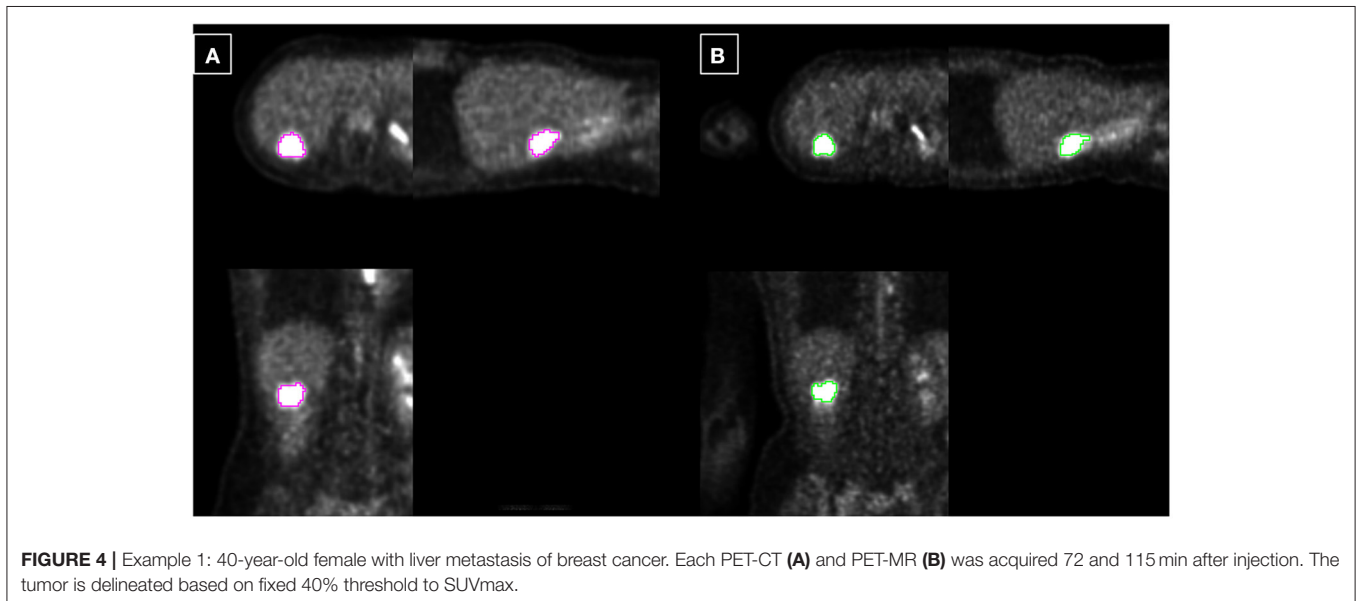


MRAC based on 4-compartment models which consist of air, lung, fat, and soft tissue. Neglecting bone tissues causes an underestimation of SUV uptake more than 10% (13, 43). The

incorrect estimation of bone tissue AC correction factors affect mostly PET signal quantification or other regions proximity to bone and this effect becomes negligible for regions at a

**TABLE 4** | The result of Bland-Altman analysis of SUV measurements between PET/CT and PET/MR.

		Mean difference (PET-MR – PET-CT)	Limits of agreement		
			Lower	Upper	
Liver	SUVmax	$-0.15 \pm 0.62$	-1.37	1.06	
	SUVmean	$-0.08 \pm 0.29$	-0.65	0.50	
	SULmax	$-0.10 \pm 0.48$	-1.03	0.83	
	SULmean	$-0.06 \pm 0.23$	-0.51	0.40	
Tumor lesion	VOI40	SUVmax	$-1.71 \pm 2.83$	-7.22	3.80
		SUVpeak	$-1.25 \pm 1.76$	-4.69	2.19
		SUVmean	$-1.06 \pm 1.87$	-4.71	2.59
		MTV	$0.35 \pm 3.55$	-6.57	7.27
	VOI50	TLG	$-2.94 \pm 13.75$	-29.76	23.88
		SUVmean	$-1.26 \pm 1.92$	-5.00	2.48
		MTV	$0.11 \pm 1.25$	-2.33	2.55
		TLG	$-1.86 \pm 7.70$	-16.88	13.15



larger distance from bone tissues. This might explain why the SUV metrics of the liver were not statistically different between the two scanners. Around the liver, there is no solid bone except for the thin rib bone, which results in maintaining the accuracy of attenuation correction. It may cause secondary critical problems in the calculation of the tumor/liver ratio or tumor delineation from the uptake of the liver. To improve upon the insufficiency of MRAC, model-based bone imposition (44), bone estimation using ZTE/UTE MRI (45, 46), and deep-learning methods (45) have been proposed. In addition, dual-tracer approach where one of the tracers is that of interest and the other may be  $^{18}\text{F}$  Sodium Fluoride,  $\text{NaF}$ , from which the bone can be segmented (20). However, other than the model-based methods, an implementation into clinical scans has yet to occur. Another factor is that the reconstruction parameters were set to be as similar as

possible, but were not identical for both scanners. The reason is that scanner software restricted users tune parameters freely (e.g., voxel resolution).

Compared to the previous MTV-reproducibility research by Groshar et al. (27), the bias of MTV in the current study was smaller (3.0 vs. 27.3%); this may be because we had a smaller scan interval ( $-12 \pm 32$  min in the current study vs.  $53 \pm 17$  min in the previous study). In contrast, the 95% limits of agreement had a larger range ( $-96.5$  and  $102.5$  vs.  $-41.7$  to  $96.2\%$ ). This might be owing to our inclusion criteria. Whereas the previous study included extremely large tumors ( $> 150$  mL), we chose to exclude tumors larger than 25 mL to maintain statistical stability. Four previous studies evaluated the reproducibility between TOF-PET-CT and TOF-PET-MR using the same commercial scanner, GE SIGNA-PET-MR; however, none of these studies performed a truly “fair”

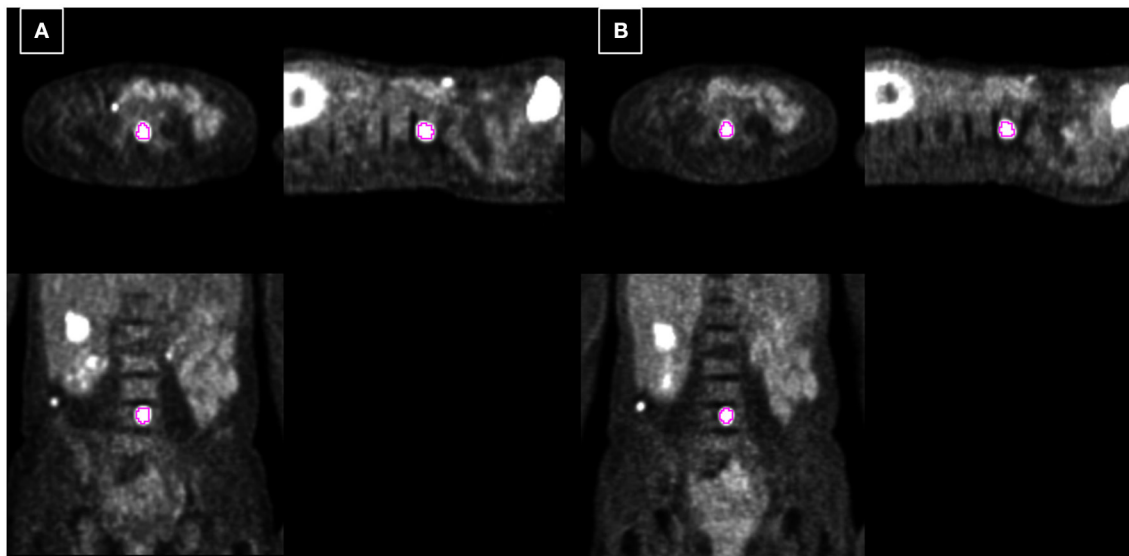


**FIGURE 5** | Example 2: 54-year-old female with spine metastasis of melanoma. Each PET-CT (A) and PET-MR (B) was acquired 73 and 48 min after injection. The tumor is delineated based on fixed 40% threshold to SUVmax.

comparison between the two scanners in terms of a fixed scan order (i.e., PET-CT following or followed by PET-MR) with a long scan interval (e.g., more than 80 min) (25, 47–49). Our study represents the first report using a random sequence of PET-CT and PET-MR acquisition, with a comparably short scan interval.

Based on our results, the SUVmax or SUVpeak metrics should be carefully considered when both PET-CT and PET-MR machines are used in follow-up or multi-center studies (50). Unlike SUVmax, SUVmean, or SUVpeak, there was no statistical difference in MTV between the two scanners. One can speculate that the tumor volume was determined by the ratio of maximum uptake and the SUV on the edge of the delineation. Therefore, if the tumor is uniformly underestimated by MRAC, the MTV does not change.

Our study has a few limitations. First, we used the 70% dose un-list PET-MR, hence evaluated data may differ from clinical data. However, the purpose of this study was to perform a fair comparison of PET-CT and PET-MR, regardless of detector sensitivity or advanced reconstruction techniques. Second, both the scan time and scan interval of PET-CT and PET-MR were not uniform. For example, some PET-CT scanned after 144 min, which was quite over from recommended protocol for PET-CT (50–70 min according to PERCIST) (51). In the delayed acquisition, the SUV-increase in tumor and SUV-decrease in benign lesion were expected, as FDG accumulation of tumor has unique characteristic, Warburg Effect, which is different from the characteristic of physiological uptake (52–56). One must consider this limitation when interpreting the current result of each liver and tumor, respectively. This limitation represents an inherent problem for a reproducibility study because repeated injection of tracer is ethically hard to justify. The same-day repeatability ruled out additional sources of quantitative error deriving from

patient habitus or the progression/regression of tumors between the two scans. Third, there might be some room to adjust the parameter of PET-MR to PET-CT, although we chose both parameters as same as possible. For further implementation of the current result into clinical research such as multi-center study, the phantom-validation applying multiple reconstruction parameters would be required. In such a case, to achieve harmonization, an automatic and secondary reconstruction of the PET-MR images which match PET-CT images would be practical (50).

## CONCLUSION

PET metrics from TOF-PET-MR had good correlation to those from TOF-PET-CT. SUVmax and SUVpeak of tumor lesions were underestimated by 16% on PET-MR. Careful consideration should be paid to the difference of the extent of underestimation between reference tissue (liver) and target tissue (tumor) when semi-quantitative parameters are measured. MTV with a % threshold can be utilized as the identical volumetric markers both on TOF-PET-CT and TOF-PET-MR.

## DATA AVAILABILITY STATEMENT

The raw data supporting the conclusions of this article will be made available by the authors, without undue reservation.

## ETHICS STATEMENT

The studies involving human participants were reviewed and approved by the Ethics Committee of University Hospital Zurich.

The patients/participants provided their written informed consent to participate in this study.

## AUTHOR CONTRIBUTIONS

TS and AT conceived the presented idea, developed the theory, performed the computations, and verified the analytical methods. MH and PV encouraged TS to investigate using this data and supervised the findings of this work.

## REFERENCES

- Ben-Haim S, Ell P. 18F-FDG PET and PET/CT in the evaluation of cancer treatment response. *J Nucl Med.* (2009) 50:88–99. doi: 10.2967/jnumed.108.054205
- Moon SH, Choi JY, Lee HJ, Son Y-I, Baek C-H, Ahn YC, et al. Prognostic value of 18F-FDG PET/CT in patients with squamous cell carcinoma of the tonsil: comparisons of volume-based metabolic parameters. *Head Neck.* (2013) 35:15–22. doi: 10.1002/hed.22904
- Choi E-S, Ha S-G, Kim H-S, Ha JH, Paeng JC, Han I. Total lesion glycolysis by 18F-FDG PET/CT is a reliable predictor of prognosis in soft-tissue sarcoma. *Eur J Nucl Med Mol Imaging.* (2013) 40:1836–42. doi: 10.1007/s00259-013-2511-y
- Hyun SH, Ahn HK, Kim H, Ahn M-J, Park K, Ahn YC, et al. Volume-based assessment by 18F-FDG PET/CT predicts survival in patients with stage III non-small-cell lung cancer. *Eur J Nucl Med Mol Imaging.* (2014) 41:50–8. doi: 10.1007/s00259-013-2530-8
- Lee JW, Cho A, Lee J-H, Yun M, Lee JD, Kim YT, et al. The role of metabolic tumor volume and total lesion glycolysis on 18F-FDG PET/CT in the prognosis of epithelial ovarian cancer. *Eur J Nucl Med Mol Imaging.* (2014) 41:1898–906. doi: 10.1007/s00259-014-2803-x
- Ogawa S, Itabashi M, Kondo C, Momose M, Sakai S, Kameoka S. Prognostic Value of total lesion glycolysis measured by 18F-FDG-PET/CT in patients with colorectal cancer. *Anticancer Res.* (2015) 35:3495–500. Available online at: <https://ar.iiarjournals.org/content/35/6/3495>
- Shao Y, Cherry SR, Farahani K, Meadors K, Siegel S, Silverman RW, et al. Simultaneous PET and MR imaging. *Phys Med Biol.* (1997) 42:1965–70. doi: 10.1088/0031-9155/42/10/010
- Fendler WP, Czernin J, Herrmann K, Beyer T. Variations in PET/MRI operations: results from an international survey among 39 active sites. *J Nucl Med.* (2016) 57:2016–21. doi: 10.2967/jnumed.116.174169
- Mayerhoefer ME, Prosch H, Beer L, Tamandl D, Beyer T, Hoeller C, et al. PET/MRI versus PET/CT in oncology: a prospective single-center study of 330 examinations focusing on implications for patient management and cost considerations. *Eur J Nucl Med Mol Imaging.* (2020) 47:51–60. doi: 10.1007/s00259-019-04452-y
- Delso G, Fürst S, Jakoby B, Ladebeck R, Ganter C, Nekolla SG, et al. Performance measurements of the Siemens mMR integrated whole-body PET/MR scanner. *J Nucl Med.* (2011) 52:1914–22. doi: 10.2967/jnumed.111.092726
- Quak E, Le Roux P-Y, Hofman MS, Robin P, Bourhis D, Callahan J, et al. Harmonizing FDG PET quantification while maintaining optimal lesion detection: prospective multicentre validation in 517 oncology patients. *Eur J Nucl Med Mol Imaging.* (2015) 42:2072–82. doi: 10.1007/s00259-015-3128-0
- Boellaard R, Delgado-Bolton R, Oyen WJG, Giammarile F, Tatsch K, Eschner W, et al. FDG PET/CT: EANM procedure guidelines for tumour imaging: version 2.0. *Eur J Nucl Med Mol Imaging.* (2015) 42:328–54. doi: 10.1007/s00259-014-2961-x
- Samarin A, Burger C, Wollenweber SD, Crook DW, Burger IA, Schmid DT, et al. PET/MR imaging of bone lesions—implications for PET quantification from imperfect attenuation correction. *Eur J Nucl Med Mol Imaging.* (2012) 39:1154–60. doi: 10.1007/s00259-012-2113-0
- Robson PM, Kaufman A, Pruzan A, Dweck MR, Trivieri M-G, Abgral R, et al. Scan-rescan measurement repeatability of

All authors discussed the results and contributed to the final manuscript.

## ACKNOWLEDGMENTS

We gratefully acknowledge Kenji Hirata, Department of Diagnostic Imaging, Graduate School of Medicine, Hokkaido University, for his advice based on the comprehensive acknowledgment of volume segmentation.

- 18F-FDG PET/MR imaging of vascular inflammation. *J Nucl Cardiol.* (2021) doi: 10.1007/s12350-021-02627-5. [Epub ahead of print].
- Robson PM, Vergani V, Benkert T, Trivieri MG, Karakatsanis NA, Abgral R, et al. Assessing the qualitative and quantitative impacts of simple two-class vs multiple tissue-class MR-based attenuation correction for cardiac PET/MR. *J Nucl Cardiol.* (2021) 28:2194–204. doi: 10.1007/s12350-019-02002-5
- Akbarzadeh A, Ay MR, Ahmadian A, Alam NR, Zaidi H. MRI-guided attenuation correction in whole-body PET/MR: assessment of the effect of bone attenuation. *Ann Nucl Med.* (2013) 27:152–62. doi: 10.1007/s12149-012-0667-3
- Dong X, Lei Y, Wang T, Higgins K, Liu T, Curran WJ, et al. Deep learning-based attenuation correction in the absence of structural information for whole-body positron emission tomography imaging. *Phys Med Biol.* (2020) 65:055011. doi: 10.1088/1361-6560/ab652c
- Torrado-Carvajal A, Vera-Olmos J, Izquierdo-Garcia D, Catalano OA, Morales MA, Margolin J, et al. Dixon-VIBE Deep Learning (DIVIDE) pseudo-CT synthesis for pelvis PET/MR attenuation correction. *J Nucl Med.* (2019) 60:429–35. doi: 10.2967/jnumed.118.209288
- Liu F, Jang H, Kijowski R, Bradshaw T, McMillan AB. Deep learning MR imaging-based attenuation correction for PET/MR imaging. *Radiology.* (2018) 286:676–84. doi: 10.1148/radiol.2017170700
- Karakatsanis NA, Abgral R, Trivieri MG, Dweck MR, Robson PM, Calcagno C, et al. Hybrid PET- and MR-driven attenuation correction for enhanced 18F-NaF and 18F-FDG quantification in cardiovascular PET/MR imaging. *J Nucl Cardiol.* (2020) 27:1126–41. doi: 10.1007/s12350-019-01928-0
- Paulus DH, Quick HH, Geppert C, Fenchel M, Zhan Y, Hermosillo G, et al. Whole-body PET/MR imaging: quantitative evaluation of a novel model-based MR attenuation correction method including bone. *J Nucl Med.* (2015) 56:1061–6. doi: 10.2967/jnumed.115.156000
- Burgos N, Jorge Cardoso M, Thielemans K, Modat M, Pedemonte S, Dickson J, et al. Attenuation correction synthesis for hybrid PET-MR scanners: application to brain studies. *IEEE Trans Med Imaging.* (2014) 33:2332–41. doi: 10.1109/TMI.2014.2340135
- Martinez-Möller A, Souvatzoglou M, Delso G, Bundschuh RA, Chef'd'hotel C, Ziegler SI, et al. Tissue classification as a potential approach for attenuation correction in whole-body PET/MRI: evaluation with PET/CT data. *J Nucl Med.* (2009) 50:520–6. doi: 10.2967/jnumed.108.054726
- Afaq A, Fraioli F, Sidhu H, Wan S, Punwani S, Chen S-H, et al. Comparison of PET/MRI With PET/CT in the evaluation of disease status in lymphoma. *Clin Nucl Med.* (2017) 42:e1–7. doi: 10.1097/RLU.0000000000001344
- Iagaru A, Mittra E, Minamimoto R, Jamali M, Levin C, Quon A, et al. Simultaneous whole-body time-of-flight 18F-FDG PET/MRI: a pilot study comparing SUVmax with PET/CT and assessment of MR image quality. *Clin Nucl Med.* (2015) 40:1–8. doi: 10.1097/RLU.0000000000000611
- Drzezga A, Souvatzoglou M, Eiber M, Beer AJ, Fürst S, Martinez-Möller A, et al. First clinical experience with integrated whole-body PET/MR: comparison to PET/CT in patients with oncologic diagnoses. *J Nucl Med.* (2012) 53:845–55. doi: 10.2967/jnumed.111.098608
- Groshar D, Bernstine H, Goldberg N, Nidam M, Stein D, Abadi-Korek I, et al. Reproducibility and repeatability of same-day two sequential FDG PET/MR and PET/CT. *Cancer Imaging.* (2017) 17:11. doi: 10.1186/s40644-017-0113-9
- Tuli A, Ayache JB, Parekh S, Thamnirat K, Chari A. Comparison of sequential PET/CT and PET/MR in previously treated multiple myeloma patients. *J Nucl Med.* (2017) 58:187. Available online at: [https://jnm.snmjournals.org/content/58/supplement\\_1/187.short](https://jnm.snmjournals.org/content/58/supplement_1/187.short)

29. Virarkar M, Ganeshan D, Gulati AT, Palmquist S, Iyer R, Bhosale P. Diagnostic performance of PET/CT and PET/MR in the management of ovarian carcinoma—a literature review. *Abdom Radiol.* (2021) 46:2323–49. doi: 10.1007/s00261-020-02847-2
30. Gao J, Huang X, Meng H, Zhang M, Zhang X, Lin X, et al. Performance of multiparametric functional imaging and texture analysis in predicting synchronous metastatic disease in pancreatic ductal adenocarcinoma patients by hybrid PET/MR: initial experience. *Front Oncol.* (2020) 10:198. doi: 10.3389/fonc.2020.00198
31. Rasmussen JH, Fischer BM, Aznar MC, Hansen AE, Vogelius IR, Löfgren J, et al. Reproducibility of (18)F-FDG PET uptake measurements in head and neck squamous cell carcinoma on both PET/CT and PET/MR. *Br J Radiol.* (2015) 88:20140655. doi: 10.1259/bjr.20140655
32. Sekine T, Burgos N, Warnock G, Huellner M, Buck A, Ter Voert EEGW, et al. Multi-atlas-based attenuation correction for brain 18F-FDG PET imaging using a time-of-flight PET/mr scanner: comparison with clinical single-atlas- and CT-based attenuation correction. *J Nucl Med.* (2016) 57:1258–64. doi: 10.2967/jnumed.115.169045
33. Davison H, ter Voert EEGW, de Galiza Barbosa F, Veit-Haibach P, Delso G. Incorporation of time-of-flight information reduces metal artifacts in simultaneous positron emission tomography/magnetic resonance imaging: a simulation study. *Invest Radiol.* (2015) 50:423–9. doi: 10.1097/RLI.0000000000000146
34. Mehranian A, Zaidi H. Impact of time-of-flight PET on quantification errors in MR imaging-based attenuation correction. *J Nucl Med.* (2015) 56:635–41. doi: 10.2967/jnumed.114.148817
35. Sekine T, Delso G, Zeimpekis KG, de Galiza Barbosa F, Ter Voert EEGW, Huellner M, et al. Reduction of 18F-FDG dose in clinical PET/MR imaging by using silicon photomultiplier detectors. *Radiology.* (2018) 286:249–59. doi: 10.1148/radiol.2017162305
36. Wollenweber SD, Ambwani S, Lonn AHR, Shanbhag DD, Thiruvankadam S, Kaushik S, et al. “Comparison of 4-class and continuous fat/water methods for whole-body, MR-based PET attenuation correction,” in *2012 IEEE Nuclear Science Symposium and Medical Imaging Conference Record (NSS/MIC)* (Anaheim, CA), 3019–25. doi: 10.1109/NSSMIC.2012.6551690
37. Boktor RR, Walker G, Stacey R, Gledhill S, Pitman AG. Reference range for intrapatent variability in blood-pool and liver SUV for 18F-FDG PET. *J Nucl Med.* (2013) 54:677–82. doi: 10.2967/jnumed.112.108530
38. Giavarina D. Understanding bland altman analysis. *Biochem Med.* (2015) 25:141–51. doi: 10.11613/BM.2015.015
39. Kitao T, Hirata K, Shima K, Hayashi T, Sekizawa M, Takei T, et al. Reproducibility and uptake time dependency of volume-based parameters on FDG-PET for lung cancer. *BMC Cancer.* (2016) 16:576. doi: 10.1186/s12885-016-2624-3
40. Orhac F, Boughdad S, Philippe C, Stalla-Bourdillon H, Nioche C, Champion L, et al. A Postreconstruction harmonization method for multicenter radiomic studies in PET. *J Nucl Med.* (2018) 59:1321–8. doi: 10.2967/jnumed.117.199935
41. Sah B-R, Stolzmann P, Delso G, Wollenweber SD, Hüllner M, Hakami YA, et al. Clinical evaluation of a block sequential regularized expectation maximization reconstruction algorithm in 18F-FDG PET/CT studies. *Nucl Med Commun.* (2017) 38:57–66. doi: 10.1097/MNM.0000000000000604
42. de Langen AJ, Vincent A, Velasquez LM, van Tinteren H, Boellaard R, Shankar LK, et al. Repeatability of 18F-FDG uptake measurements in tumors: a metaanalysis. *J Nucl Med.* (2012) 53:701–8. doi: 10.2967/jnumed.111.095299
43. Andersen FL, Ladefoged CN, Beyer T, Keller SH, Hansen AE, Højgaard L, et al. Combined PET/MR imaging in neurology: MR-based attenuation correction implies a strong spatial bias when ignoring bone. *Neuroimage.* (2014) 84:206–16. doi: 10.1016/j.neuroimage.2013.08.042
44. Oehmigen M, Lindemann ME, Gratz M, Kirchner J, Ruhlmann V, Umutlu L, et al. Impact of improved attenuation correction featuring a bone atlas and truncation correction on PET quantification in whole-body PET/MR. *Eur J Nucl Med Mol Imaging.* (2018) 45:642–53. doi: 10.1007/s00259-017-3864-4
45. Leynes AP, Yang J, Wiesinger F, Kaushik SS, Shanbhag DD, Seo Y, et al. Zero-Echo-Time and Dixon Deep Pseudo-CT (ZeDD CT): direct generation of pseudo-CT images for Pelvic PET/MRI attenuation correction using deep convolutional neural networks with multiparametric MRI. *J Nucl Med.* (2018) 59:852–8. doi: 10.2967/jnumed.117.198051
46. Sekine T, Ter Voert EEGW, Warnock G, Buck A, Huellner M, Veit-Haibach P, et al. Clinical evaluation of zero-echo-time attenuation correction for brain 18F-FDG PET/MRI: comparison with atlas attenuation correction. *J Nucl Med.* (2016) 57:1927–32. doi: 10.2967/jnumed.116.175398
47. Minamimoto R, Igaru A, Jamali M, Holley D, Barkhodari A, Vasanaawala S, et al. Conspicuity of malignant lesions on PET/CT and simultaneous time-of-flight PET/MRI. *PLoS One.* (2017) 12:e0167262. doi: 10.1371/journal.pone.0167262
48. Queiroz MA, Delso G, Wollenweber S, Deller T, Zeimpekis K, Huellner M, et al. Dose optimization in TOF-PET/MR compared to TOF-PET/CT. *PLoS One.* (2015) 10:e0128842. doi: 10.1371/journal.pone.0128842
49. Vontobel J, Liga R, Possner M, Clerc OF, Mikulicic F, Veit-Haibach P, et al. MR-based attenuation correction for cardiac FDG PET on a hybrid PET/MRI scanner: comparison with standard CT attenuation correction. *Eur J Nucl Med Mol Imaging.* (2015) 42:1574–80. doi: 10.1007/s00259-015-3089-3
50. Aide N, Lasnon C, Veit-Haibach P, Sera T, Sattler B, Boellaard R. EANM/EARL harmonization strategies in PET quantification: from daily practice to multicentre oncological studies. *Eur J Nucl Med Mol Imaging.* (2017) 44:17–31. doi: 10.1007/s00259-017-3740-2
51. Wahl RL, Jacene H, Kasamon Y, Lodge MA. From RECIST to PERCIST: evolving considerations for PET response criteria in solid tumors. *J Nucl Med.* (2009) 50(Suppl 1):122S–50S. doi: 10.2967/jnumed.108.057307
52. Sanz-Viedma S, Torigian DA, Parsons M, Basu S, Alavi A. Potential clinical utility of dual time point FDG-PET for distinguishing benign from malignant lesions: implications for oncological imaging. *Rev Esp Med Nucl.* (2009) 28:159–66. doi: 10.1016/S0212-6982(09)71360-6
53. Pietrzak AK, Kazmierska J, Marszalek A, Cholewinski W. Evaluation of physiologic and abnormal glucose uptake in palatine tonsils: differential diagnostics with sequential dual-time-point 2-deoxy-2-[18F]FDG PET/CT. *Q J Nucl Med Mol Imaging.* (2020) 64:299–306. doi: 10.23736/S1824-4785.18.03065-0
54. Koppol WH, Bounds PL, Dang CV. Otto Warburg’s contributions to current concepts of cancer metabolism. *Nat Rev Cancer.* (2011) 11:325–37. doi: 10.1038/nrc3038
55. Houshmand S, Salavati A, Segtnan EA, Grupe P, Høilund-Carlson PF, Alavi A. Dual-time-point imaging and delayed-time-point fluorodeoxyglucose-PET/computed tomography imaging in various clinical settings. *PET Clin.* (2016) 11:65–84. doi: 10.1016/j.cpet.2015.07.003
56. Shimizu K, Okita R, Saisho S, Yukawa T, Maeda A, Nojima Y, et al. Clinical significance of dual-time-point 18F-FDG PET imaging in resectable non-small cell lung cancer. *Ann Nucl Med.* (2015) 29:854–60. doi: 10.1007/s12149-015-1013-3

**Conflict of Interest:** GD is an employee of GE Healthcare. GW is an employee of Pmod Inc.

The remaining authors declare that the research was conducted in the absence of any commercial or financial relationships that could be construed as a potential conflict of interest.

**Publisher’s Note:** All claims expressed in this article are solely those of the authors and do not necessarily represent those of their affiliated organizations, or those of the publisher, the editors and the reviewers. Any product that may be evaluated in this article, or claim that may be made by its manufacturer, is not guaranteed or endorsed by the publisher.

Copyright © 2022 Tanaka, Sekine, ter Voert, Zeimpekis, Delso, de Galiza Barbosa, Warnock, Kumita, Veit Haibach and Huellner. This is an open-access article distributed under the terms of the Creative Commons Attribution License (CC BY). The use, distribution or reproduction in other forums is permitted, provided the original author(s) and the copyright owner(s) are credited and that the original publication in this journal is cited, in accordance with accepted academic practice. No use, distribution or reproduction is permitted which does not comply with these terms.